Soft Electrically Actuated Quadruped (SEAQ) – Integrating a Flex Circuit Board and Elastomeric Limbs for Versatile Mobility

Xiaonan Huang, Kitty Kumar, Mohammad K. Jawed, Zisheng Ye, and Carmel Majidi

Abstract—Like their natural mammalian and reptilian counterparts, legged soft robots require robust walking dynamics and untethered functionality in order to swiftly maneuver through unstructured environments. Progress in this domain requires careful selection of soft limb actuators and integration of power and control electronics into a soft robotics platform capable of biologically-relevant locomotion speeds without dependency on external hardware. We demonstrate this with an untethered soft palm-sized, 25g soft electrically actuated quadruped (SEAQ; Fig. 1(a)) that is capable of crawling at a maximum speed of 0.56 body length per second (3.2cm/s) and making 90 degree turns in two complete gait cycles (~5s). The robot is composed of a flexible printed circuit board and electrically-powered soft limbs that contain shape memory alloy (SMA) wires inserted between pre-stretched layers of a soft, thermally-conductive elastomer. Its versatile mobility and robust dynamics are demonstrated by its ability to walk on a variety of surfaces – including inclines, rocky and granular surfaces, and steps that are over half the robot height – and maintain continuous forward locomotion through confined space or after being dropped from an elevated height. In addition to these locomotion studies, we perform an experimental study on the blocking force of a single actuator to provide independent support for the feasibility of untethered soft robot walking with SMA-based actuation.

***Index Terms*—Soft robotics, actuators, shape memory alloy**

I. Introduction

UNTETHERED robots that match the ability of natural organisms to freely swim, undulate, walk over long distances, and cohabitate with biological life represent a central goal of the bio-inspired robotics community [1]–[5]. Such robots are of great interest for space exploration [6], [7], defense [8]–[10], security, surveillance tasks [11]–[13], and search and rescue operations [14]–[16]. For terrestrial applications, limb-like motion has been widely studied with robots that are piecewise rigid [17]–[19] or composed of non-elastic or inextensible materials [20]–[24]. It is, however, challenging to achieve legged-locomotion in an untethered soft-bodied robot. Such systems require mechanically robust limbs that have adequate bending stiffness to support forces necessary to overcome the weight of the robot and propel it forward. However, the limbs must also be soft enough so that the robot can be squeezed into confined spaces or walk through a tight opening [25]. Thus, the soft limb actuator must be carefully selected in order to satisfy two seemingly competing properties: high mechanical compliance and load-bearing force capacity. Moreover, the untethered soft robot must contain lightweight on-board electronics that can power the limbs to actuate at frequencies necessary for the robot to walk in dry conditions at speeds approaching those of natural limbed organisms.

The fastest untethered legged soft robots to date has been the untethered Pneu-net quadruped reported in [25], which has a walking speed of 0.5cm/s (~0.01 blps). Although the speed of it is below the range of walking speeds for natural organisms or other bio-inspired robotic systems, that work represents an important milestone in the field by demonstrating that it is possible to engineer an untethered soft quadruped with all of its supporting hardware on-board. To achieve faster locomotion that approaches the walking speeds of natural organisms (~1-10 blps [26]), we have chosen to replace pneumatic actuation with actuators that can be stimulated electronically so that they can be directly powered and controlled with portable, lightweight batteries and circuitry. In particular, we selected shape memory alloy (SMA) wire, since it can be powered with electrical current, has a high work density (~10 J/cm^3), and can generate large forces (~200 MPa) in a short interval (<0.2s) [27]–[29]. Furthermore, they can swiftly switch between a compliant and a stiff state when electrically activated and deactivated, respectively. For these reasons, SMAs have been popular in fast moving soft robots like the GoQBot [30], which is capable of near-ballistic motion. Recently, there have been attempts to engineer legged soft robots with SMA actuation [31]–[33],

Manuscript received: September 10, 2018; revised December 25, 2018; accepted January 30, 2019. This paper was recommended for publication by Editor Kyu-Jin Cho upon evaluation of the Associate Editor and Reviewers' comments. This work was supported by Army Research Office (Grant #: W911NF-16-1- 0148; Program Manager: Dr. Samuel Stanton) and National Aeronautics and Space Agency (NASA ECF; Grant #: NNX14AO49G; Technical Contact: Dr. Bill Bluethmann).

All authors are with the Soft Machines Lab, Department of Mechanical Engineering, Carnegie Mellon University, Pittsburgh, PA 15213 USA (e-mail: xiaonanh@andrew.cmu.edu).

M. K. Jawed is now with Mechanical & Aerospace Engineering Department, University of California, Los Angeles, CA 90095 USA (e-mail: khalidjm@seas.ucla.edu).

C. Majidi is also with Robotics Institute, Carnegie Mellon University, Pittsburgh, PA 15213 USA (e-mail: cmajidi@andrew.cmu.edu).

Digital Object Identifier (DOI): see top of this page

This article has been accepted for publication in a future issue of this journal, but has not been fully edited. Content may change prior to final publication. Citation information: DOI 10.1109/LRA.2019.2903856, IEEE Robotics and Automation Letters

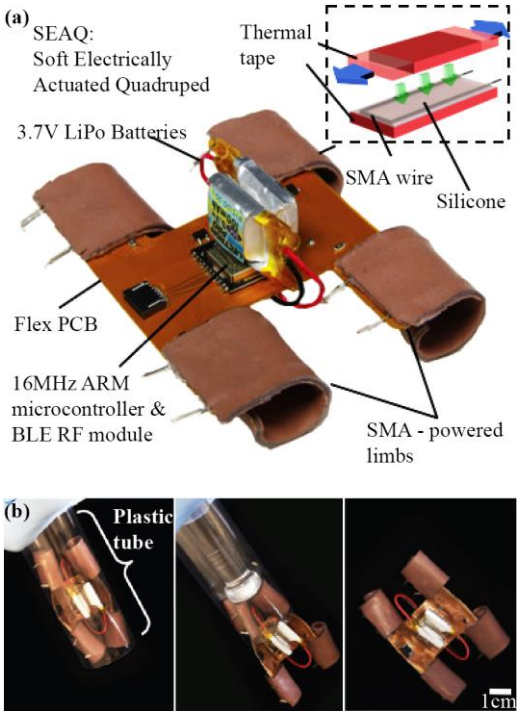

Fig. 1. (a) Components of SEAQ; inset shows the layup for the SMA-powered limbs. (b) Photographs showing SEAQ can be squeezed in a tube and automatically deployed after taken out.

although such implementations are tethered and rely on external hardware for power or actuation. Nonetheless, because of their high work density and stiffness-tuning properties, SMAs are promising for "cutting the cord" and creating untethered soft robots with biologically-relevant walking speed [34].

Here we present an untethered soft electrically actuated quadruped (SEAQ) (Fig. 1(a)) that has a weight of 25g and walks with a maximum speed of 3.2 cm/s (0.56 blps; Supplementary Video S1). In terms of blps, this robot is ~50x faster than the previous attempt at an untethered walking soft quadruped and is within the range of walking speeds for natural organisms and similarly-sized semi-rigid robots such as RoACH [20] and HAMR3 [24]. SEAQ exhibits a unique combination of elastic deformability, biologically-relevant walking speed, and untethered functionality and can potentially serve as a testbed for studying the dynamics of limbed soft robots. The tight integration of compliant materials and on-board electronics is demonstrated in Fig. 1(a), which shows the construction of the 5.7× 7.4 cm^2 palm-sized quadruped. The four electrically-activated limbs are fabricated out of SMA wires that are sandwiched between two layers of elastomer coated soft, thermally conductive rubber (Fig. 1(a) inset) [35]. Since it is primarily composed of soft and flexible material, SEAQ is collapsible and can be squeezed into a narrow (3.7cm diameter) plastic tube without damage (Fig. 1(b)).

The robot walks with a trot-like locomotion gait that enables walking up an incline (Fig. 2(a); Supplementary Video S2), over a variety of surfaces such as rocky terrain (Fig. 2(b); Supplementary Video S3) and on granular media (e.g. poppy seeds, Fig. 2(c); see Supplementary Video S4), through a confined space (1.7cm height; Fig. 2(d); Supplementary Video S5) and over a 8 mm tall step (i.e. slightly greater than half the robot height; Fig. 2(e); see also Supplementary Video S6). Additionally, the mechanical compliance and tight integration of on-board electronics also contribute to enhanced robustness and impact resistance. As shown in Fig. 2(f), SEAQ is capable of continuous motion before and after falling from a 1m height (Supplementary Video S7). Although enabling biologically-relevant walking speeds, the trot-like locomotion is not intended to match natural walking gaits – see [36] for a more complete discussion of natural legged locomotion.

The primary contribution of this work is to demonstrate that with appropriate material selection, hardware integration, and operation, it is possible to design untethered soft robots that can walk at speeds (~0.1-1 blps) and in conditions (smooth, confined, granular) similar to natural limbed locomotion. This represents a significant milestone in the nascent field of soft

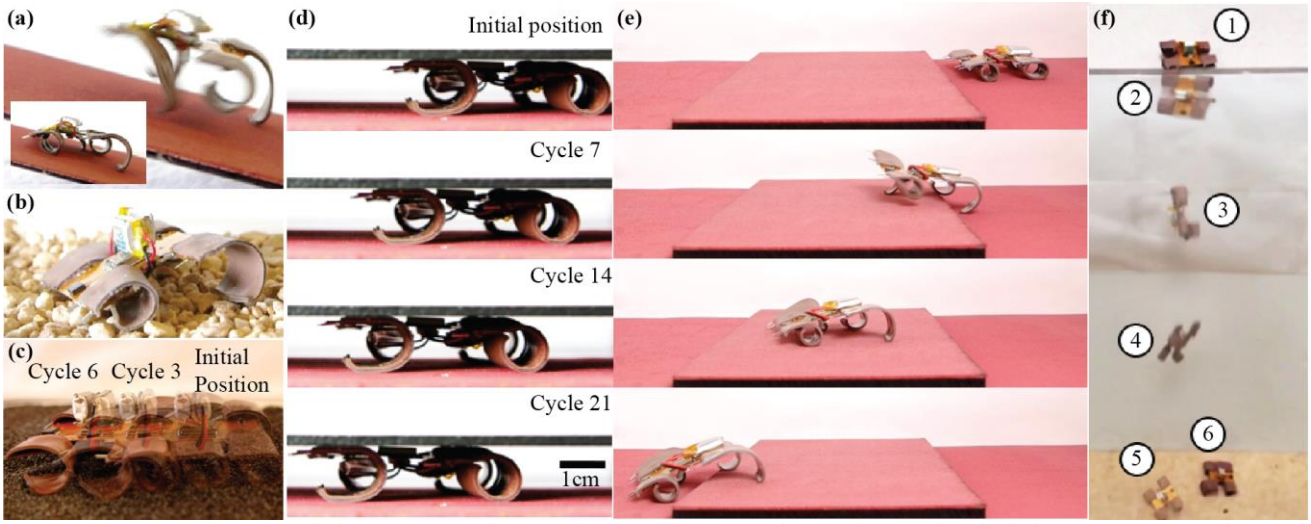

Fig. 2. With four soft and compliant limbs, SEAQ can walk on a wide variety of terrains without needing to adjust the limb orientation or gait. Photographs showing SEAQ (a) climbing a 15˚ incline; (b) walking over a rocky terrain composed of small stones and (c) granular surface; (d)navigating through a tight opening of 17mm in height and (e) walking over an 8 mm step, i.e. slightly greater than half of the robot height. (f) Composite of video frames showing SEAQ falling from a 1m height without losing function.

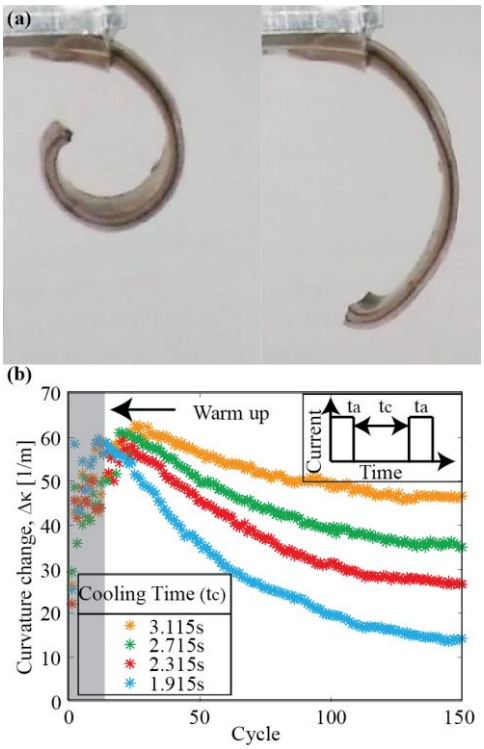

Fig. 3. (a) High speed video frames of an actuator in a relaxed (left) and activated state (right). (b) Plot of curvature changes for 150 cycles under various cooling time. Signal sequence is shown as an inset.

robotics since it shows that such systems are capable of dynamic, load-bearing motion and biologically-relevant mobility without dependency on bulky external hardware.

II. Design Overview

Refering to Fig. 1(a), the quadruped is composed of a flexible printed circuit board (PCB) with a processor (16 MHz ARM M0) and Bluetooth radio transceiver (RFD22301, RFDUINO), a pair of lithium polymer (LiPo) batteries (3.7V, 100mAh; Lectron), and four naturally-curled limbs. As shown in the inset, each limb-actuator consists of a U-shaped nickle-titanium (Nitinol) shape memory wire (length = 123mm, diameter = 0.3mm, A_s = 70˚C, A_f = 90˚C; Dynalloy) sandwiched between two rectangular sheets of thermally conductive rubber (55×22×0.5mm, 70×60×0.5mm; H48-2, T-Global). The longer sheet is stretched to 150% of its original length prior to bonding and cut to the dimension of the smaller sheet after bonding. This introduces residual strain (ε) that causes the limb to curl upwards and adopt a natural C- shaped curvature. It takes ~0.09s for the SMA to reach its start transition temperature and ~0.15s to reach its finish transition temperature when actuated by the robot's flex PCB and batteries at room temperature.

The onboard processor and transistors (AO3416, Alpha & Omega Semiconductor) manage the electrical current delivered from a pair of LiPo batteries that are connected in series to the SMA-embedded limbs. The flex PCB and batteries have a total weight of 8.1g and delivers 4.0-4.3A of current to the limbs at 105-180ms intervals. When an impulse of current is delivered to the limb, it transitions from a curled shape to a relatively straight shape and then recoils to its naturally curled shape owing to the antagonistic force generated from the prestretched layer. The current is delivered to one of the rear limbs first and then delivered to the front one that is diagonally opposite. Likewise, the other pair is activated after a short period to enable the activated limbs to cool down. The symmetrical gait is repeated to propel the robot forward.

III. Fabrication, Integration and Characterization

A. Flex PCB Fabrication and Integration

The top and bottom layouts of the circuit are printed on two separate pieces of copper sheets (Pyralux 8515R) using a wax printer (XERO 8580), where the wax ink covers the pads vias and traces on the circuit. Next, we dip the copper sheets in a solution of HCl and H_2O_2 (1:2 by volume) to etch the exposed copper. After cleaning the sheets, we remove the wax with a brush and acetone solution and connect the top and bottom layers by inserting tiny rivet through the vias and soldering them together. Then we put Kapton tapes on both sides of the circuit with soldering pads exposed. Finally, we solder all the IC components to the flex PCB board.

B. Actuator Fabrication

We create an actuator that is (i) soft enough to adapt to variable terrains and external impacts but also load-bearing to hold the weight of the electronics, (ii) capable of swiftly generating adequate force to propel the robot forward and (iii) capable of fast actuation and deactivation. This is accomplished by inserting a piece of pre-bent SMA wire (0.3mm in diameter, Dynalloy) between a pre-stretched and unstretched layer of thermally conductive elastomer (0.5 mm thick; H48-2, T-Global). The SMA wire is bent into a loop that is 13mm in width and 55mm in length. The thermal conductivity, tensile strength and hardness of the material are 2.2W/m·K, 7 kgf/cm^2, and Shore 10A, respectively. The SMA wire has a resistance of about 12.2 Ω/m at room temperature and the resistance of each actuator is ~1.5 Ω. The prestretched thermal tape gives the actuator a curled shape so that it can act as a load-bearing limb. It also provides an antagonistic force that overcomes the mechanical hysteresis of the SMA wire and allows the limb to rapidly recoil.

The actuator fabrication process starts by cutting the thermal tape with a CO2 laser (30W VLS 3.50; Universal Laser Systems) into two rectangular pieces with dimensions of 55×22mm and 70×37mm respectively. Next, the two-part prepolymer is prepared by mixing part A and part B (Ecoflex 00-30, Smooth-On) at a 1:1 ratio by mass in a planetary centrifugal mixer (AR-100, THINKY). We use a thin film applicator (ZUA 200, Zehntner Testing Instruments) to apply a 0.2mm thick coating of uncured Ecoflex 00-30 on the smaller of the two rectangular pieces. The elastomer is then partially cured at 50ºC for 7 minutes in the oven. Next, a pre-bent SMA wire is placed on top of the partially cured Ecoflex layer and an additional 0.4mm thick film of uncured Ecoflex 00-30 layer is coated on top. In the meantime, a thin layer of uncured Ecoflex 00-30 is applied on top of the prestretched tape, which is stretched (50%

This article has been accepted for publication in a future issue of this journal, but has not been fully edited. Content may change prior to final publication. Citation information: DOI 10.1109/LRA.2019.2903856, IEEE Robotics and Automation Letters

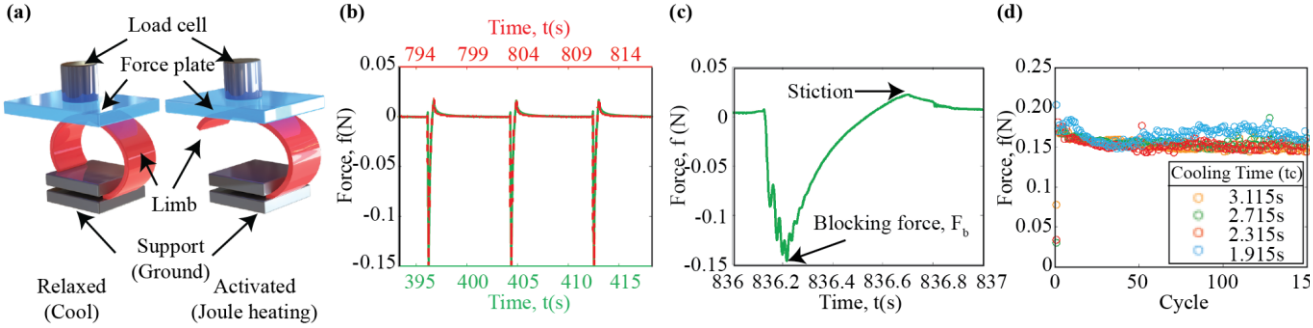

Fig. 4. (a) Schematic of the experimental setup for blocking force (F_b) measurement. (b) Measured contact force (f) versus time (t) after 50 (green solid) and 100 (red dashed) cycles of actuation. The overlap between the f-t curves suggests repeatable actuation with negligible influence on the actuation force from the functional fatigue (i.e. irrecoverable deformation) as a result of cyclical mechanical and thermal loading of SMA wire. (c) Zoomed-in plot of a single actuation showing the magnitude of the blocking force during actuation and stiction measured during relaxation. (d) Plot of blocking force for 150 cycles.

strain for the limbs used for this robot) using a linear stretcher (A150602-S1.5, Velmex). Both tapes with Ecoflex 00-30 layers are half-cured at 50°C for 7 minutes and then clamped together with two binder clips. The silicone elastomer between the thermal layers is half-cured in order to enable bonding but also enough mechanical support to prevent the SMA wire from moving during fabrication. The sandwich structure (two pieces of tape with the SMA wire sandwiched in Ecoflex) is then cured fully at 50°C for 10 minutes. Finally, we cut out along the outline of the smaller tape using scissors to obtain the final robot limb.

C. *Actuator Characterization*

The mobility of SEAQ depends on the structure and response of each limb, which are defined by the limb curvature and reaction force, respectively. To better understand these relationships, we begin with an in-depth characterization of the individual actuators to quantify their flexural response and blocking force over repeated cycles. To examine the repeated flexural response, we actuate the actuator with an activation time $t_a = 0.105$s with a current of 4.0-4.3A and cool it down for a cooling time t_c for 150 cycles. Correspondingly, the actuator transitions from a compliant curled state (Fig. 3(a), left) to a rigid less curled state (Fig. 3(a), right). We treat the shape of the actuator as a circular arc with a uniform curvature. Using image frames, we extract the maximum actuated curvature within a cycle followed by the non-actuated curvature at the end of the cycle. Then we take the difference of these two curvature values as the curvature change at each cycle and present it in Fig. 3(b) for 150 repeated cycles at different cooling times t_c (1.915s, 2.315s, 2.715s, 3.115s). The actuator is powered by a 7.4V power supply and controlled by a microcontroller (RFD22301; RFduino) and transistor (A03416; Alpha & Omega Semiconductor). The actuation scheme is shown in the inset of Fig. 3(b). As shown in Fig. 3(b), the curvature change $\Delta\kappa$ starts to increase in the first ~10-25 cycles ("warm up" phase, shaded area in Fig. 3(b)) as the heat starts to accumulate within the structure, leading to an increase of the baseline temperature. This accumulation causes the soft martensite crystalline structure to transition to a rigid austenite phase and results in a more straight shape during actuation. Since the baseline temperature is still below the austenite starting transition temperature (A_s), the crystalline structures stay at the martensite phase resulting in a high bending curvature of the actuator at the end of each cycle.

As the baseline temperature exceeds A_s, $\Delta\kappa$ starts to decrease with subsequent cycles and then reaches a steady state after ~100 cycles for longer cooling time (e.g. $t_c = 3.115$s) as the baseline temperature stabilizes. However, the curvature change continues to decrease dramatically for shorter cooling time (e.g. $t_c = 1.915$s) since the continuously increasing baseline temperature prevents the more rigid austenite crystalline structure from recovering to the soft martensite phase. In this way, the antagonistic force from the prestretched layer cannot bend the rigid SMA wire back to the initial curled shape resulting in reduced curvature change.

SEAQ exploits the change in shape of the actuated limbs to exert a force on the ground and overcome frictional force and gravity to propel the robot forward. To evaluate this force, we fix a rigid force plate to a 10N load cell mounted on the top grip of a motorized materials testing system (Instron 5969) and clamp an actuator to the bottom grip (Fig. 4a). We adjust the distance between the force plate and the actuator such that the actuator just touches the force plate with a negligible amount of force in the relaxed state. To examine the blocking force output, we actuate the actuator for $t_a = 0.15$s and deactivate it for $t_c = 8.0$s for 102 repeated cycles with the same circuit used in the characterization of the flexural response. As the actuator tries to straighten out, it is blocked by the rigid plate and the blocking force is recorded by the Instron. For the cyclic loading, we use the same electronic setup and control scheme to measure the blocking force output over repeated cycles.

Fig. 4(b) overlays a snapshot of the force signal from 393s-418s (~ 50 cycles, green, solid curve) with a snapshot of the force signal from 792s-817s (~100 cycles, red, dotted curve). In both cases, the maximum force in each cycle is 0.15 N. The nearly identical values of the force in both the curves emphasize the repeatability of the actuator for at least 100 cycles. In Fig. 4(c), the force measurement over a quarter of the actuation cycle has been shown, which is essentially a zoomed-in view of Fig. 4(b) near the peak force. A positive force of about 0.02N can be seen that may be attributed to the stiction between the actuator and the force plate. The absolute

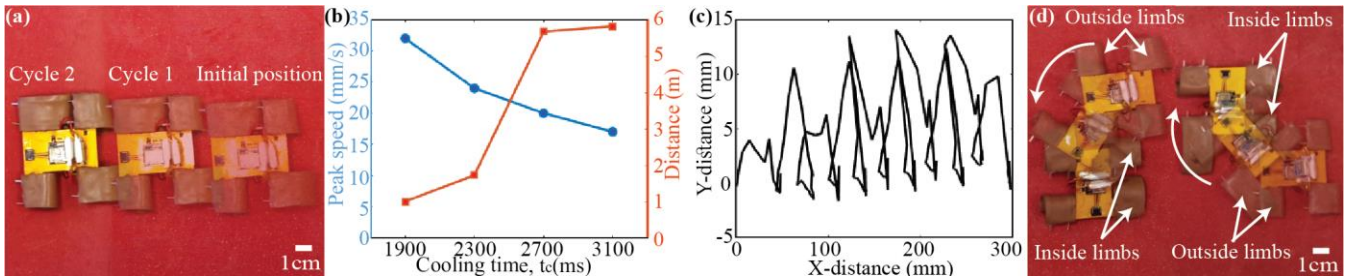

Fig. 5. (a) Composite of video frames showing SEAQ traveling over two body lengths in two cycles. (b) Plot showing speed and travel distance versus cooling time (tc). (c) Plot showing trajectory of the center of mass during several walking cycles. (d) Composite of videos frames showing SEAQ turning both left and right in two cycles.

value of the peak force in each cycle, approximately 0.15N in this case, is defined as the blocking force, F_b. We repeat the experiment for four times with four actuators and acquire an average blocking force of 0.14N. For the cyclic test, blocking force increases rapidly in the first couple of cycles and then stabilizes around a steady state value between 0.15–0.17N as shown in Fig. 4(d). This is because the stiffness barely changes once the maximum temperature during actuation exceeds A_f (temperature for complete transition to the austenite). The higher blocking force when t_c = 1.915s may be caused by the softening effect of the thermally conductive tape at higher temperature.

IV. Soft Robot Implementation

In this section, we present a more detailed quantitative study of SEAQ locomotion on a flat terrain. Based on the characterization in Sec. III, we have established that the individual limbs can be designed to support adequate curvature change (18 – 65m^{-1}), force (0.15 to 0.17N), and activation frequencies (0.31 to 0.5Hz) for soft quadruped locomotion. To validate the ability to use these limbs for untethered soft robot locomotion, we performed a series of locomotion experiments for forward walking, turning, centroid trajectory, and cost of transport (COT) analysis. Together with the operational conditions shown in Fig. 2 and Movies S1–S8, these studies demonstrate the possibility of engineering untethered soft robots that walk at speeds which approach those of natural limbed organisms and maneuver through various terrains.

A. Locomotion Experiments

For the alternating trot-like gait, the robot translates an entire body length with each full gait cycle (Fig. 5(a)). This straight-line locomotion is achieved by first actuating the rear left limb (Limb 4) in order to shift the center of mass of the robot forward. During this time, the front right limb (Limb 2) rolls forward and is actuated right after the Limb 4 so that most of the thrusting force is supplied to move the robot in the forward direction. The next pair of limbs (front left limb (Limb 1) & rear right limb (Limb 3)) are actuated after the time gap of t = 0.8s. This interval gives time for Limbs 2 & 4 to cool down so that they begin to curl inwards just as Limbs 1 & 3 are being actuated.

With the above actuation sequence, SEAQ is capable of continuous walking at a peak speed of 3.2cm/s (0.56 blps, ~1 body length per cycle, Fig. 5(a)) over a distance of 1m before the limbs overheat (Fig. 5(b)). However, longer distances of up to 5.82m can be traveled with a pair of onboard fully charged 3.7V LiPo batteries by increasing the cooling time to t_c = 3.115s, which corresponds to the walking speed of 1.7 cm/s (0.3 blps) (Fig. 5(b)). A cooling time of less than 1.915s is inadequate for the limbs to cool down and fully curl back, which results in poor locomotion. For maximized travel distance, a cooling time of approximately 3.115s is used since it prevents the limbs from overheating. SEAQ locomotion in a straight line on a smooth surface at various actuation frequencies is presented in Supplementary Video S1. For all measurements, a current of ~4.0-4.3A is supplied to each limb by a pair of 3.7V LiPo batteries that connected in series for t_a = 0.105s. Based on the characterization in Sec. III, these operational conditions enable the actuator to exert a force between 0.14N and 0.2N. In general, we observe that providing a relatively large electric current in a short time results in a higher operational frequency [28] compared with supplying low electric current for a longer time [29].

Referring to Fig. 5(c), we analyzed the motion of SEAQ by tracking the trajectory of the center of mass (Tracker 4.97). The center of mass is shown to move both in the horizontal (X) and vertical (Y) directions. As the robot moves forward, its center of mass moves up by approximately 15mm with each step. This vertical displacement is necessary in order to give a pair of limbs the clearance required to curl inwards while the other pair is being actuated. In the case of a t_c = 3.115s cooling time, the robot moves forward by approximately 50 mm, followed by a backward motion of 18 mm for each gait cycle. Moreover, we observe that the length of this backward motion decreases with decreasing cooling time since it is interrupted by the next actuation cycle.

As shown in Fig. 5(d), the quadruped can make turns by increasing the actuation time of the limbs on the outside to 0.13s and limiting the inside ones to 0.095s. This enables the outside limbs to completely actuate and move faster than the inside ones while the inside ones only actuate enough to lift the robot up to create space for the outside ones to curl back. With the above actuation sequence for the inner and outer limbs, it takes two complete gait cycles (~5s) to turn the quadruped by 90 degrees with a radius of ~5cm (0.88 body length) (Fig. 5(d), Supplementary Video S8).

B. Cost of Transport

During walking, a current of ~4.0-4.3A is delivered to the limbs of SEAQ using a pair of on-board 3.7V LiPo batteries. When the limbs are activated with a t_a = 0.105s heating and t_c = 3.115s cooling time, the robot walks at a speed of 0.3 blps (1.7cm/s) for a distance of 5.82m on a full battery charge. This corresponds to a cost of transport (CoT) of 786, which is very high on account of the poor electrical-to-mechanical energetic conversion efficiency of the SMA wires [27]. We define cost of transport (CoT) as $W/mg\Delta d$, where Δd is the travel distance of the robot and W is the amount of energy required for the robot traveling for Δd. We calculate W as I^2Rt where I is the current flow through the actuator, R (~1.5 ohm) is the resistance of the actuator, and t is the total time that the actuators are activated. Here, we assume the current flow through the actuators is constant, although in reality the current will gradually decrease as the battery is discharged. We also ignore the energy consumption in the electronics (N-MOSFETs etc.), which will contribute to an even greater COT. A maximum walking speed of 0.56 blps is obtained when the cooling time is reduced to 1.915s. However, for this relatively short cooling time, the robot can only travel a distance of 1m before the limbs overheat (CoT = 527.5).

V. Discussion and Future Work

We have presented a 5.7cm long, 25g untethered soft robot with four electrically-activated flexural limbs. With a maximum speed of 3.2cm/s (0.56 blps), the robot is capable of approaching the walking speed of natural organisms. This improvement over past efforts in untethered soft robots is enabled by adopting a fully electronic system for actuation, control, and power. The robot is capable of making a 90- degree turn in two complete gait cycles (~5s) with a turning radius of approximately 5 cm and can walk on a rocky surface, granular matter, and through a confined space. The components of the robot, i.e., body, limbs, and control board, are incorporated into an integrated materials architecture that is elastically compliant and mechanically robust.

A. Untethered Functionality

Electrically-controlled operation represents a key feature of the untethered soft quadruped. This enables the robot to be controlled with flexible lightweight hardware and a miniaturized on-board power supply.

With further progress in soft materials engineering and hardware miniaturization, we anticipate future implement-ations of untethered soft robot that achieve dynamic mobility through other sources of power and actuator stimulation. These include pneumatics, hydraulics, magnetic field, light, and high voltage electrostatics. Although they rely on different actuator technologies, the design of such soft robots can build on the following insights gained from the present study: (i) Actuators need to be load bearing but also mechanically compliant so that they are capable of both holding the weight of the electronics and body of the robot and adapting to variable terrains and external impact. (ii) Rapid transition from a compliant to rigid state can contribute to faster locomotion; i.e. we provide a large current (4.0-4.3A) in a short period (0.105-0.18s) instead of providing a lower current in a longer period. (iii) The versatile mobility enabled by a robot's compliance and flexibility can be preserved by selecting an electronics board that is lightweight and flexible.

B. Opportunity for Improvement & Future Work

While SEAQ exhibits a relatively high walking speed compared to other untethered soft robots, body-lengths-per-second represents just one of several metrics that are important in comparing aspects of robot locomotion. Another important metric is the operation time for continuous locomotion on a single battery charge. SEAQ can walk continuously for 6 minutes, which is comparable to the ~9 minutes of continuous walking that is possible with RoACH [20]. However, this is significantly less than the ~1.6 hour operation time for the Pneu-net quadruped reported in [25]. Achieving greater duration requires further refinements to the design or locomotion gait that allow for added batteries or decreased limb activation frequency without reducing the robot's average walking speed.

Another opportunity for improvement is the energy efficiency for continuous locomotion. The limited range and high CoT that we calculated arise from the dependency on Joule heating to power the soft robot limbs. In general, thermal actuation consumes significant power and requires adequate time to cool down. One way to improve speed and travel distance is to make further improvements to the heat management system, e.g. use elastomers with higher thermal conductivity [37], [38]. Another method is with feedback control schemes that use measurements from embedded strain and temperature sensors that are incorporated in the elastomeric structure. Lastly, CoT and energy efficiency, along with other important metrics of robot performance, could be improved through the use of non-thermal methods of actuation. This could potentially include emerging techniques like combustion-driven actuation through fuel decomposition [39] or bio-hybrid actuators powered with natural muscle tissue [40].

Future efforts could also focus on further characterization of robot deformability and ability to withstand dynamic loadings and impact. By being largely constructed from elastomers, such soft robots could match or exceed the robust performance of motor-driven compliant robots like DASH, which can withstand 28m falls [22]. However, we believe that there could be connection issues between the flex board and rigid IC components if the robot is subject to extreme impact loads or excessive mechanical disturbances. Another area of interest is the use of computational tools to simulate soft robot locomotion in order to inform design and gait selection. In particular, such modeling tools could be used to explore the role of limb elasticity and deformation in the energetic cost of locomotion and help identify ways to improve CoT through elastic energy storage and power amplification [41].

VI. Conclusion

In closing, we show that it is possible to achieve biologically-relevant walking speeds in an untethered soft robot when a fully electronic approach is adopted. Compared to a pneumatically-powered soft robot [25], [42], the tight integration of materials, control electronics, power, and actuation in an electronic soft robot allows for reduced hardware complexity, size, and weight. Although we focused on a quadruped design, the materials architecture presented here can be generalized to a broad range of robot designs including caterpillar-inspired segmented robots and single- limbed jumpers. In this respect, the current work could potentially serve as a template for engineering untethered soft robots with electrically-powered limbs. The construction and electrical operation of these robots can be informed by design insights obtained from characterizing the flexural properties of the individual limbs. Such future implementations could also be engineered to address remaining challenges and limitations. These include fundamental tradeoffs between walking speed, total duration, actuator cool down time, total battery capacity, and robot payload (for a more complete overview of factors in soft robotics design, see [34], [43]– [48]). Opportunities for improvement might also include soft flexible batteries that could be incorporated into the limbs as well as novel methods for more rapid heat dissipation and cooling.

References

[1] A. J. Ijspeert, "Biorobotics: Using robots to emulate and investigate agile locomotion," *Science,* vol. 346, no. 6206, pp. 196–203, 2014.

[2] K. Autumn *et al.*, "Robotics in scansorial environments," vol. 5804, p. 291, 2005.

[3] J. Aguilar *et al.*, "A review on locomotion robophysics: the study of movement at the intersection of robotics, soft matter and dynamical systems," *Rep. Prog. Phys.*, vol. 79, no. 110001, p. 35, 2016.

[4] Y. Li, B. Li, J. Ruan, and X. Rong, "Research of mammal bionic quadruped robots: A review," in *Proc. Int. Conf. Robot., Autom.. Mechatronics,* 2011, pp. 166–171.

[5] S. Zimmerman and A. Abdelkefi, "Review of marine animals and bioinspired robotic vehicles: Classifications and characteristics," *Progress in Aerospace Sciences*, vol. 93. pp. 95–119, 2017.

[6] T. Fong and I. Nourbakhsh, "Interaction challenges in human - robot space exploration," *ACM Interact.*, vol. 12, no. 2, pp. 42-45, 2005.

[7] D. Goldberg *et al.*, "A distributed layered architecture for mobile robot coordination: Application to space exploration," in *Proc. Int. NASA Workshop on Planning and Scheduling for Space*, 2002.

[8] E. Sloan, "Robotics at war," *Survival (Lond).*, vol. 57, no. 5, pp. 107-120, 2015.

[9] P. W. Singer, "Military robots and the future of war," *New Atl.*, vol. 23, no. c, pp. 25–45, 2009.

[10] P. Lin, G. Bekey, and K. Abney, "Autonomous Military Robotics: Risk, Ethics, and Design," 2008.

[11] H. Lee, W.-C. Lin, C.-H. Huang, and Y.-J. Huang, "Wireless indoor surveillance robot," *SICE Annu. Conf. 2011*, pp. 2164 – 2169, 2011. "

[12] G. Song, K. Yin, Y. Zhou, and X. Cheng, "A surveillance robot with hopping capabilities for home security," *IEEE Trans. Consum. Electron.*, vol. 55, no. 4, pp. 2034–2039, 2009.

[13] X. Wu, H. Gong, P. Chen, Z. Zhi, and Y. Xu, "Intelligent household surveillance robot," in *IEEE Int. Conf. on Robot. Biomim.,* 2008, pp. 1734–1739.

[14] C. Wright *et al.*, "Design of a modular snake robot," in *IEEE Int. Conf. on Intell. Robot. Syst.*, 2007, pp. 2609–2614.

[15] T. Kamegawa, T. Yamasaki, H. Igarashi, and F. Matsuno, "Development of the snake-like rescue robot 'KOHGA,'" in *Proc. IEEE Int. Conf. Robot. Autom.*, 2004.

[16] K. Kamikawa, T. Arai, K. Inoue, and Y. Mae, "Omni-Directional Gait of Multi-Legged Rescue Robot," in *Proc. IEEE Conf. Robot. Autom.*, 2004.

[17] S. Seok *et al.*, "Design principles for energy-efficient legged locomotion and implementation on the MIT Cheetah robot," *IEEE/ASME Trans. Mechatronics*, vol. 20, no. 3, pp. 1117–1129, 2015.

[18] R. Altendorfer *et al.*, "RHex: A biologically inspired hexapod runner," *Auton. Robots*, vol. 11, no. 3, pp. 207–213, 2001.

[19] U. Saranli, M. Buehler, and D. E. Koditschek, "RHex: A Simple and Highly Mobile Hexapod Robot," *Int. J. Rob. Res.*, vol. 20, no. July, pp. 616–631, 2001.

[20] A. M. Hoover, E. Steltz, and R. S. Fearing, "RoACH: An autonomous 2.4g crawling hexapod robot," in *Proc. IEEE/RSJ Int. Conf. Intell. Robots Syst.,* 2008, pp.26–33.

[21] D. W. Haldane, K. C. Peterson, F. L. Garcia Bermudez, and R. S. Fearing, "Animal-inspired design and aerodynamic stabilization of a hexapedal millirobot," *Proc. - IEEE Int. Conf. Robot. Autom.*, pp. 3279–3286, 2013.

[22] P. Birkmeyer and R. S. Fearing, "DASH: A resilient high-speed 15g hexapedal robot," in *IEEE/RSJ Int. Conf. Intell. Robots Syst.,* 2009, pp. 418–419.

[23] S. Kim, J. E. Clark, and M. R. Cutkosky, "ISprawl: Design and tuning for high-speed autonomous open-loop running," *Int. J. Rob. Res.*, vol. 25, no. 9, pp. 903–912, 2006.

[24] A. T. Baisch, C. Heimlich, M. Karpelson, and R. J. Wood, "HAMR3: An autonomous 1.7g ambulatory robot," in *IEEE Int. Conf. Intell. Robots Syst*, 2011, pp. 5073–5079.

[25] M. T. Tolley *et al.*, "A Resilient, Untethered Soft Robot," *Soft Robot.*, vol. 1, no. 3, pp. 213–223, 2014.

[26] N. Meyer-Vernet and J.-P. Rospars, "How fast do living organisms move: Maximum speeds from bacteria to elephants and whales," *Am. J. Phys.*, vol. 83, no. 8, pp. 719–722, 2015.

[27] J. Mohd Jani, M. Leary, A. Subic, and M. A. Gibson, "A review of shape memory alloy research, applications and opportunities," *Materials and Design*, vol. 56. pp. 1078–1113, 2014.

[28] Z. Wang, G. Hang, J. Li, Y. Wang, and K. Xiao, "A micro-robot fish with embedded SMA wire actuated flexible biomimetic fin," *Sensors Actuators, A Phys.*, vol. 144, no. 2, pp. 354–360, 2008.

[29] Motzki, T. Gorges, M. Kappel, M. Schmidt, G. Rizzello, and S. Seelecke, "High-speed and high-efficiency shape memory alloy actuation," *Smart Mater. Struct.*, vol. 27, no. 7, p. 075047, 2018.

[30] H.-T. Lin, G. G. Leisk, and B. Trimmer, "GoQBot: a caterpillar- inspired soft-bodied rolling robot," *Bioinspir. Biomim.*, vol. 6, no. 2, p. 026007, 2011.

[31] H. Jin *et al.*, "A starfish robot based on soft and smart modular structure (SMS) actuated by SMA wires," *Bioinspir. Biomim.*, vol. 11, no. 5, p. 056012, 2016.

[32] S. Mao *et al.*, "Gait study and pattern generation of a starfish-like soft robot with flexible rays actuated by SMAs," *J. Bionic Eng.*, vol. 11, no. 3, pp. 400–411, 2014.

[33] H. Jin, E. Dong, M. Xu, C. Liu, G. Alici, and Y. Jie, "Soft and smart modular structures actuated by shape memory alloy (SMA) wires as tentacles of soft robots," *Smart Mater. Struct.*, vol. 25, no. 8, p. 85026, 2016.

[34] S. I. Rich, R. J. Wood, and C. Majidi, "Untethered soft robotics", *Nat. Electron.*, vol. 1, no. 2, pp. 102–112, 2018.

[35] X. Huang *et al.*, "Highly dynamic shape memory alloy actuator for fast moving soft robots", *Adv. Mater. Technol.*, 1800540, 2019.

[36] R. M. Alexander, *Principles of Animal Locomotion*. Princeton Univeristy Press.

[37] M. D. Bartlett *et al.*, "High thermal conductivity in soft elastomers with elongated liquid metal inclusions," *Proc. Natl. Acad. Sci.*, vol. 114, no. 9, pp. 2143–2148, 2017.

[38] N. Kazem, T. Hellebrekers, and C. Majidi, "Soft Multifunctional Composites and Emulsions with Liquid Metals," *Adv. Mater.*, vol. 29, no. 27. 2017.

[39] N. W. Bartlett *et al.*, "A 3D-printed, functionally graded soft robot powered by combustion," *Science*, vol. 349, no. 6244, pp. 161–165, 2015.

[40] C. Cvetkovic *et al.*, "Three-dimensionally printed biological machines powered by skeletal muscle," *Proc. Natl. Acad. Sci.*, vol. 111, no. 28, pp. 10125–10130, 2014.

[41] T. J. Roberts and E. Azizi, "Flexible mechanisms: the diverse roles of biological springs in vertebrate movement," *J. Exp. Biol.*, 2011.

[42] R. F. Shepherd *et al.*, "Multigait soft robot," *Proc. Natl. Acad Sci.*, vol. 108, no. 51, pp. 20400–20403, 2011.

[43] S. Kim, C. Laschi, and B. Trimmer, "Soft robotics: A bioinspired evolution in robotics," *Trends in Biotechnology*, vol. 31, no. 5. pp. 287–294, 2013.
[44] D. Rus and M. T. Tolley, "Design, fabrication and control of soft robots," *Nature*, vol. 521, no. 7553, pp. 467–475, 2015.
[45] D. Trivedi, C. D. Rahn, W. M. Kier, and I. D. Walker, "Soft robotics: Biological inspiration, state of the art, and future research," *Appl. Bionics Biomech.*, vol. 5, no. 3, pp. 99–117, 2008.
[46] C. Majidi, "Soft Robotics: A Perspective—Current Trends and Prospects for the Future," *Soft Robot.*, vol. 1, no. 1, pp. 5–11, 2014.
[47] C. Laschi, B. Mazzolai, and M. Cianchetti, "Soft robotics: Technologies and systems pushing the boundaries of robot abilities," *Sci. Robot.*, vol. 1, no. 1, p. eaah3690, 2016.
[48] R. Pfeifer, M. Lungarella, and F. Iida, "The challenges ahead for bio-inspired 'soft' robotics," *Commun. ACM*, vol. 55, no. 11, p. 76, 2012.